The International Journal of Advanced Manufacturing Technology (2021) 117:3515–3527
https://doi.org/10.1007/s00170-021-07926-2

ORIGINAL ARTICLE

A novel global sensitivity analysis method for vital geometric errors of five-axis machine tools

Jinwei Fan[1] · Peitong Wang[1] · Xingfei Ren[1]

Received: 17 February 2021 / Accepted: 22 August 2021 / Published online: 30 August 2021

Abstract

Geometric error is one of the important errors that affect the machining of five-axis machine tools and how to identify th8e vital geometric error is effective for compensation. For this reason, the global sensitivity analysis of geometric errors for five-axis machine tools is an effective means to find the vital geometric error items that affect the machining accuracy of machine tools. However, it is difficult to deal with the higher order items of error parameter coupling in the global sensitivity analysis. In this paper, a novel global sensitivity analysis method for vital geometric error based on multi-body theory and truncated Fourier expansion is proposed. First, multi-body system (MBS) and homogeneous transformation matric (HTM) methods are used to establish the position error of the machine tool. Then, the output value of the error parameter is represented as the amplitude of the truncated Fourier series and the global sensitivity index is represented by the ratio of its amplitude variance to the total function variance through normalization processing. Moreover, the global sensitivity analysis method is presented to calculate the sensitivity index of each geometric error parameter and the vital geometric error parameters have been identified. Finally, an experiment on compensating for vital geometric error parameters is performed and the experimental results show that the proposed method is feasible and accurate.

Keywords Machine tool · Geometric error · Sensitivity analysis · Multi-body system · Truncated Fourier

1 Introduction

In the modern manufacturing industry, the five-axis CNC machine tools are increasingly used in the precision machining of complex surfaces for their high productivity and flexibility [1, 2]. Thus, the improvement of machining accuracy has attracted much attention. However, many factors affect the of the machining accuracy of the machine tools, such as geometric errors, thermal errors, cutting-force induced errors, and tool wear errors. In these errors, the geometric errors, which are caused by inaccuracies built-in components and assembly errors, form one of the biggest sources of inaccuracy [3]. Compensating geometric errors is an important means of improving machining accuracy. Among many geometric errors, each one has different effects on machining accuracy. Thus, a practical sensitivity analysis of geometric errors is an important way to compensate errors. In the past few years, many scholars have conducted in-depth research on geometric error compensation to search an effective analysis method to improve the machining accuracy. Bryan reported the use of magnetic ball bars for measuring linear axis motion errors. Since then, various groups have applied this method to measure geometric errors of machines [4]. Tsutsumi et al. proposed an algorithm to identify eight specific geometric errors for a five-axis machine tool using the ball bar [5]. Ibaraki et al. presented an efficient calibration method to identify location errors and position-dependent geometric errors for a five-axis machine tool using R-test [6]. In order to improve the accuracy of the integrated geometric errors of the machine tool, Fu et al. proposed a novel error model based on D-H method [7]. In recent years, multi-body system method has been widely used in geometric error modeling of machine tools [8–10]. The MBS method has the characteristics of good universality, clear physical definition, and convenient calculation. Compared with the D-H method, the homogeneous

✉ Peitong Wang
504789981@qq.com

[1] College of Mechanical Engineering & Applied Electronics Technology, Beijing University of Technology, Beijing 100124, People's Republic of China

transmission matrix (HTM) is applied in the MBS method to represent the coordinate transformation between each rigid body. Considering the nonlinearity and uncertainty of error, data fitting is suitable for error modeling based on measurement data [11–13]. In this paper, the MBS and the HTM are adopted for the geometric error modeling.

On the basis of these theories made by predecessors, the position error model of five-axis machine tools can be mapped. However, it is difficult to deal with these error parameters to acquire the sensitive error parameters due to the high nonlinearity of the position error. Zhang et al. applied the MDRM method into the GSA of machine tools to identify the key geometric errors [14]. In order to better analyze the motion accuracy and error design of machine tools, Tang et al. proposed a comprehensive sensitivity analysis method for 3-DOF parallel machine based on the probability model [15]. Huang et al. conducted error design based on the interval analysis method and pointed out that over estimate of errors on boundary was brought by this method [16]. Xing et al. proposed a method of machine tool accuracy monitoring based on position errors, vector similarity measurement, and exponential weighted moving average control char [17]. Li et al. proposed a sensitivity analyses for the five-axis machine tool volume error conducted by defining the new sensitivity indices [18]. As can be observed in the abovementioned studies, Sobol, Morris, and single error derivation methods have been widely used in many applications. Among these methods, how to choose a simple method to identify the vital error parameters that affect the machining accuracy is the key to solve the error compensation and precision design. However, these GSA requires a large amount of calculation and computer simulations, which will take a lot of time in this analysis process.

Therefore, in order to find out essential geometric errors for machine tools efficiently, an accurate and quick sensitivity analysis method is urgently needed to identify the vital geometric errors. This paper proposes a general sensitivity analysis to calculate the error sensitivity index which is an important reflection of the error affecting the position error of machine tools. Then, the each sensitivity index of geometric errors is calculated and the vital geometric errors are identified. Finally, the machining accuracy of the machine tool is improved significantly by compensating the vital geometric errors.

The structure of this paper is arranged as follows. In section 2, the position error model of five-axis machine tool is obtained based on MBS theory. In section 3, the error sensitivity analysis based on truncated Fourier expansion is established. In section 4, the experiments are conducted and the results show that the global sensitivity method is effective and feasible. In section 5, the paper is summarized.

2 Position error model

2.1 Description of geometric errors

Geometric errors come from assembly errors and manufacturing errors of machine parts which are reflected on each axis of straightness errors, angular errors, and squareness errors. There are 21 geometric error parameters for three translational axis, including 18 position-dependent geometric error (PDGE) parameters and 3 position-dependent geometric error (PIGE) parameters. Taking the X-axis as an example shown in Fig. 1, it has 6 degrees of freedom in space. Thus, when it moves, it will generate PDGE parameters ($\sigma_x(x)$, $\sigma_y(x)$, $\sigma_z(x)$, $\varepsilon_x(x)$, $\varepsilon_y(x)$, $\varepsilon_z(x)$) as shown in Fig. 1. Among them, $\sigma_x(x)$, $\sigma_y(x)$, $\sigma_z(x)$ represent the straightness errors along the X-axis in the X, Y and Z directions respectively and $\varepsilon_x(x)$, $\varepsilon_y(x)\varepsilon_z(x)$represent the angle error around the X, Y and Z directions, respectively. Since the five-axis machine possesses five motion axis, there are 30 PDGE parameters in total. In addition, because of the assembly relationship between each axis of the machine tool, there are 7 PIGE parameters (S_{xy}, S_{xz}, S_{yz}, S_{xb}, S_{xc}, S_{yc}, S_{zb}). As illustrated in Fig. 2, the PIGE parameter S_{xy} represents squareness error between X-axis and Y-axis, and S_{xz}represents squareness error between X-axis and Z-axis. Thus, the five-axis machine tool has 37 geometric errors in total as shown in Table 1.

2.2 Structure of the five-axis machine tool

The structure of five-axis machine tool is usually divided into three types, such as RTTTR, TTTRR, and RRTTT respectively. The letter T represents the translational axis and the letter R represents the rotary axis. This paper takes a planer milling machine as an example as shown in Fig. 3; this structure of five-axis machine tool is TTTRR, which consists of a workpiece (0), X-axis (1), Y-axis (2), Z-axis (3), C-axis (4), and B-axis (5). The stroke of the translational axis is expressed as X × Y × Z = 5000 × 2000 × 500 mm. The stroke of the B-axis is [− 30°, 30°] and the stroke of the C-axis is [− 180°, 180°].

Table 1 Geometric error parameter

Numbers	Geometric error parameters
1,2,3,4,5,6	σ_X(x), σ_y(x), σ_z(x), ε_x(x), ε_y(x), ε_z(x)
7,8,9,10,11,12	σ_x(y), σ_y(y), σ_z(y), ε_x(y), ε_y(y), ε_z(y)
13,14,15,16,17,18	σ_x(z), σ_y(z), σ_z(z), ε_x(z), ε_y(z), ε_z(z)
19,20,21,22,23,24	σ_x(B), σ_y(B), σ_z(B), $\varepsilon_x(B)$, $\varepsilon_y(B)$, $\varepsilon_z(B)$
25,26,27,28,29,30	σ_x(C), σ_y(C), σ_z(C), $\varepsilon_x(C)$, $\varepsilon_y(C)$, $\varepsilon_z(C)$
31,32,33,34,35,36,37	S_{xy}, S_{xz}, S_{yz}, S_{xb}, S_{xc}, S_{zb}, S_{yc}

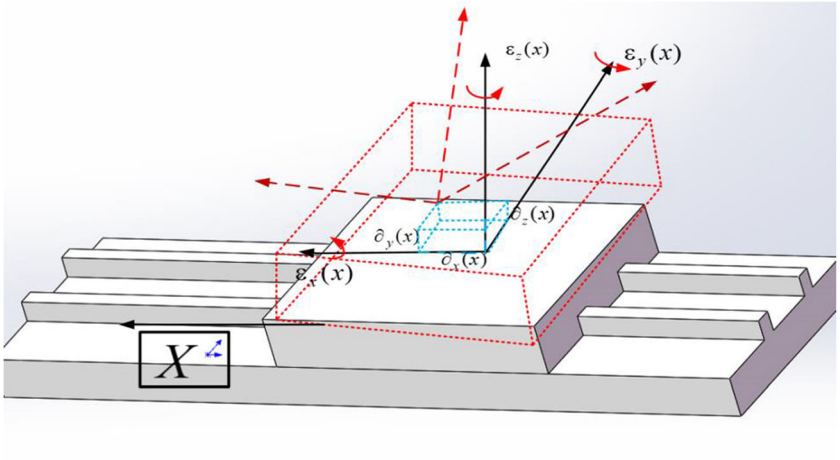

Fig. 1 Position-dependent geometric error on the X-axis

Compared to a three-axis machine tool, the geometric errors caused by the two rotation axis of a five-axis machine tool should be taken into consideration when modeling the position error of five-axis machine tool.

2.3 Position error model

The position error of tool points is caused by the deviation between the actual tool position and the ideal tool position. In order to describe the motion relationship between adjacent bodies clearly, the machine tool topology needs to be established according to MBS. As shown in Fig. 4, the motion of each adjacent body of the machine tool can be expressed by error parameter matrix according to HTM. Thus, it is necessary to calculate the tool's actual point and ideal point. Because of the manufacturing and assembly errors of each part of the machine tool, it will generate the corresponding geometric error in the position and movement of each axis.

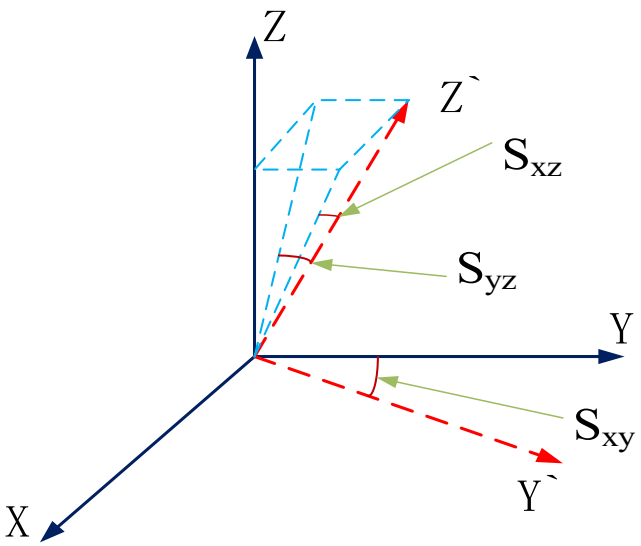

Fig. 2 Position-independent geometric error

Thus, the ideal motion matrix and actual motion matrix of the machine tool are respectively expressed as

$$[T_{ij}]_i = [T_{ij}]_p [T_{ij}]_s \quad (1)$$

$$[T_{ij}]_a = [T_{ij}]_p [T_{ij}]_{pe} [T_{ij}]_s [T_{ij}]_{se} \quad (2)$$

Where$[T_{ij}]_a$, $[T_{ij}]_p$, $[T_{ij}]_i$and$[T_{ij}]_s$ represent the actual motion transformation matrix, position error transformation matrix, ideal motion transformation matrix, and motion error transformation matrix between two adjacent bodies i and j, respectively.

Thus, the actual and ideal position equations of the tool can be obtained in the workpiece system, according to the MBS and HTM. The formula for each adjacent body is shown in Appendix 1 Tables 4 and 5. Assuming that the initial position of tool $[\boldsymbol{r}_t] = (0, 0, -L, 1)^T$ is known, the actual position (P_a) and ideal position (P_i) of the tool can be expressed as Eqs. ((3) , (4)), respectively.

$$P_a = [T_{01}]_a [T_{12}]_a [T_{23}]_a [T_{34}]_a [T_{45}]_a [r_t] \quad (3)$$

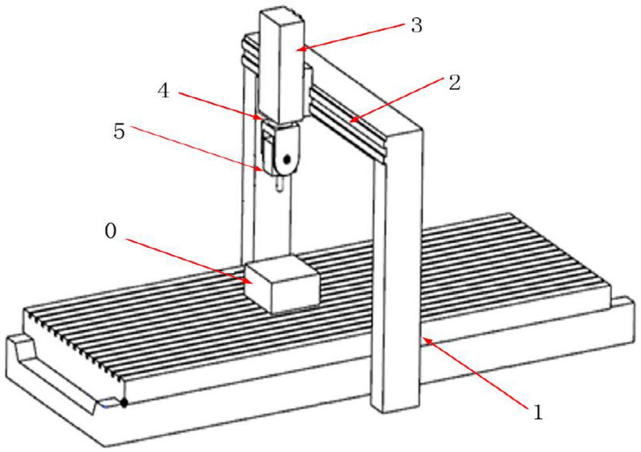

Fig. 3 Five-axis machine tool schematic diagram

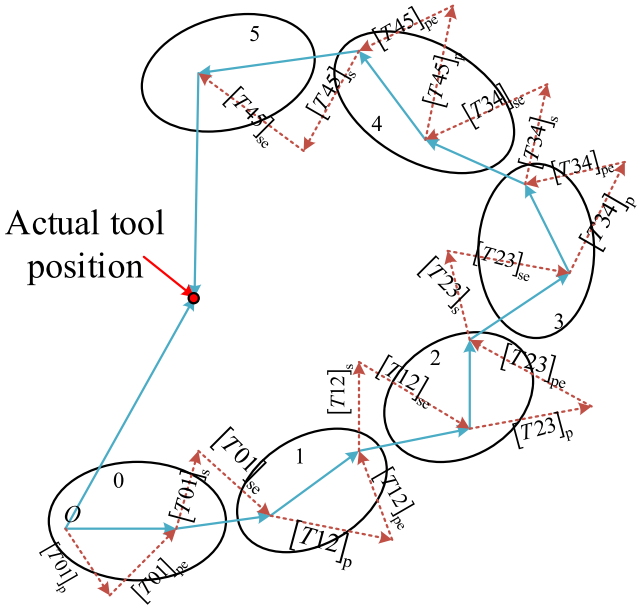

Fig. 4 Topological structure of machine tool

$$P_{\mathrm{i}} = [T_{01}]_{\mathrm{i}}[T_{12}]_{\mathrm{i}}[T_{23}]_{\mathrm{i}}[T_{34}]_{\mathrm{i}}[T_{45}]_{\mathrm{i}}[r_t] \tag{4}$$

Where L represents the length of tool and the matrix $[T_{ij}](i=1,2..6,j=2,3\ldots7)$ represents the position transformation relationship between two adjacent bodies. $[T_{ij}]_a$and $[T_{ij}]_i$ represent the product of the matrices movement of the cutting tool the actual and ideal positions relations of two adjacent bodies respectively.

Based on the topological structure of the five-axis machine tool, it is obvious that in the process of calculation of the actual movement of the cutting tool. Thus, the position error (P_e = (P_{ex}, P_{exy}, P_{ez}, 0)) of the machine tool can be expressed as

$$P_{\mathrm{e}} = P_{\mathrm{a}} - P_{\mathrm{i}} \tag{5}$$

3 Global sensitivity index model

The sensitivity analysis of position error in cutting point with regard to each error component can be made, which will be helpful in the precision design of a machine tool according to the position error model in the above section. Thus, sensitivity coefficients are introduced to express the degree which error parameters have greater affect in the given workspace. However, the position error P_e contains many error parameters and the coupling of error parameters. In order to fully consider the contribution of each geometric error parameter on the total error, an error sensitivity analysis model is mapped where the error parameters can be regarded as the input and the position error P_e can be regarded as the output. In this paper, the proposed method provides a new way of computing and reduce the number of calculation. The specific steps are as follows: Fourier series expansion is used to characterize the geometrical error parameters, which transforms the global sensitivity analysis results into the solution of Fourier amplitude. Finally, the geometric error parameters of machine tool are solved by the position error model and the amplitude is determined.

3.1 Global sensitivity model based on truncated Fourier

As shown in Table 1, there are 37 geometric error parameters which contain 30 position-dependent geometric errors and 7 position-independent geometric errors in a five-axis machine tool. According to Ref. [12], the position-independent geometric errors generated by assembly are considered a constant value. Therefore, the following analysis is based on the position-independent geometric errors compensated. P_{ek} (k=x,y,z) is set to be the integrated error function f(t) and t_i represents independent variable for all geometric errors.

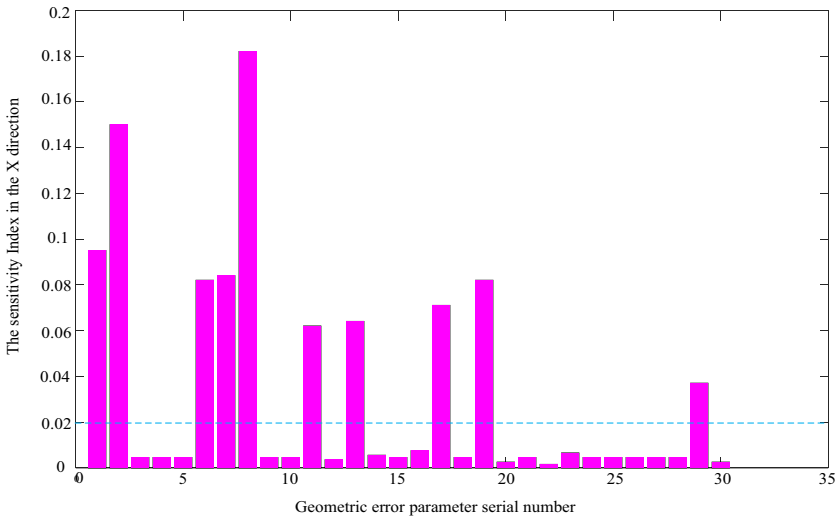

Fig. 5 Global sensitivity index in the X direction

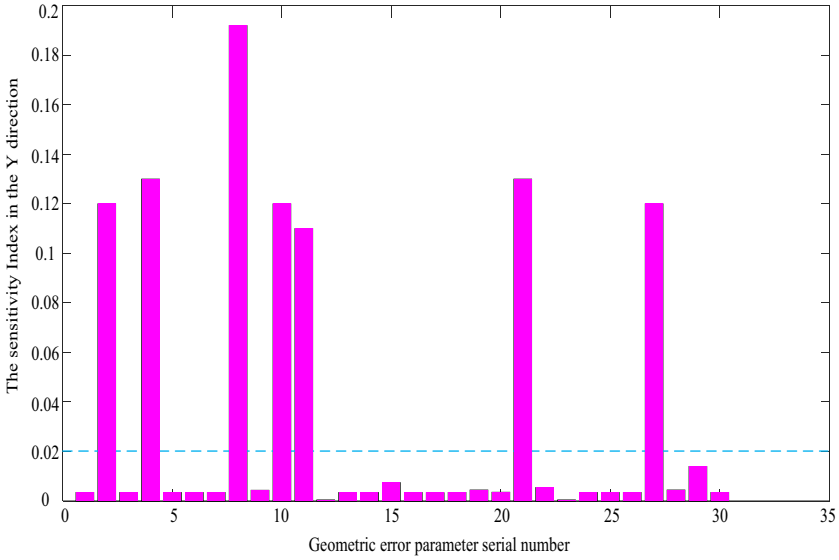

Fig. 6 Global sensitivity index in the Y direction

$$P_{ek} = f(t) = f(x_1, x_2, x_3 \ldots x_{30}) \tag{6}$$

$$t_i \in \{\sigma_x(X), \sigma_y(X), \sigma_z(X), \varepsilon_x(X) \ldots \varepsilon_z(C)\} \tag{7}$$

According to Ref.[16], the position errors are not only random and continuous but also related to the position of motion. These position-dependent geometric errors fulfill Dirichlet boundary conditions; hence, the position-dependent geometric errors can be represented by a series of Fourier. The geometric errors function can be expressed as

$$f(t) = \sum_{j=1.3.5..}^{N} A_j \sin\left(\frac{2\pi t}{\lambda_j}\right) \tag{8}$$

Therefore, the coefficient A_j can be expressed as

$$A_j = \frac{2}{N+1} \sum_{i=1}^{N_t} f(t_i) \sin\left(\frac{2\pi t_i}{\lambda_j}\right) \tag{9}$$

Where t represents independent variable of geometric error parameter and $\lambda_j$represents the wavelength of the error parameter. In (0,2π), there is an uniform interval N_t ($N_t = M\lambda_{min} + 1$) that M is usually selected as 4 and λ_{min} is the smallest wavelength in $\{\lambda_j\}$. Each wavelength λ in $\{\lambda_j\}$ is linearly independent. So, there is a set of integers $\{r_j\}$ that makes the members of set $\{\lambda_j\}$ linearly independent.

$$\begin{cases} \sum_{i=1}^{30} r_j \lambda_j \neq 0 \\ j \in B = [1, 2, 3, \ldots N_t] \\ t_k = \dfrac{2k - N_t - 1}{2N_t}, k \in D = [1, 2, 3, \ldots N_t] \\ F = B - \left\{\dfrac{N_t + 1}{2}\right\} \end{cases} \tag{10}$$

The Fourier frequency spectrum curve is defined as τ

$$\tau = A_j^2 \tag{11}$$

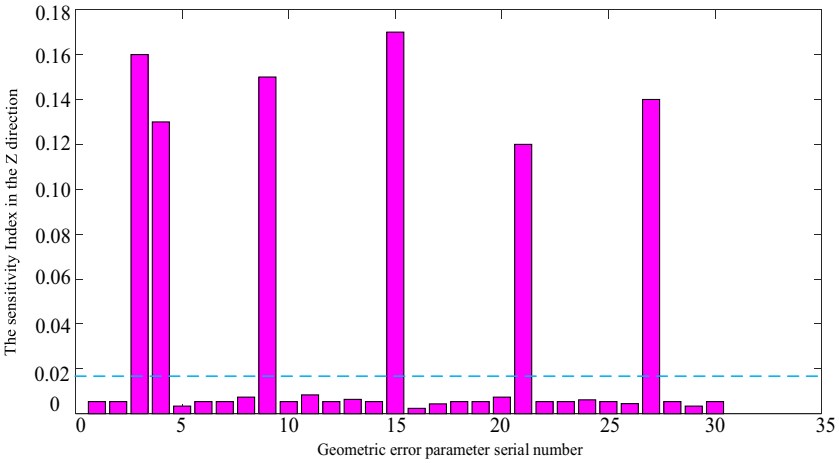

Fig. 7 Global sensitivity index in the Z direction

The variance of the model caused by the change of the parameter input can be expressed as the spectrum curve of the parameter.

$$V_i = \sum \tau \lambda_j = \sum_{n=1}^{M} A_{j=n}^2 \tag{12}$$

The variance of the output of the sensitivity analysis model caused by each input error parameter can be expressed as

$$V = \sum_{t_1=1}^{30} V_{t_1} + \sum_{t_1 \neq t_2}^{30} V_{t_1 t_2} + \cdots + \sum V_{t_1 t_2 \ldots t_{30}} = \sum_{F} \tau = \sum_{j=1}^{\frac{N_t+1}{2}} \tau_j \tag{13}$$

Where t_1, t_2 and t_{30} represent each of the different error parameters in the set {t}.

In order to describe the contribution of error parameters on position error more clearly and quantitatively, each geometric error parameter is normalized (the unit of straightness errors and angle errors are 1 um and 1 urad, respectively). The contribution of each error parameter on the machining error is expressed by the first-order sensitivity index (S_i)

$$S_i = \frac{V_i}{V} \tag{14}$$

The sensitivity index is the ratio of the variance of the sensitivity model output changed by the input error parameter to the variance of the errors, which is regarded as the local sensitivity index. By calculating the sensitivity index for each error, the first-order sensitivity index is more intuitive to express the influence of the transformation of input parameters on the output error. The first-order sensitivity index S_m simply reflects the contribution of single geometric error item on output while it cannot truly reflect the output of the coupling effect of parameter i and other error parameters. Thus, the global sensitivity (Sti) index is introduced.

Table 2 Tool point parameter on region H

	x/mm	y/mm	z/mm	c/°	b/°
1	3329.38	654.61	446.72	170.52	− 10.59
2	3330.63	656.03	446.51	169.44	− 10.84
3	3331.82	657.38	446.30	168.35	− 11.10
4	3332.93	658.67	446.08	167.25	− 11.35
5	3333.92	659.89	445.87	166.15	− 11.58
6	3334.78	661.07	445.66	165.03	− 11.80
7	3335.50	662.24	445.47	163.90	− 11.99
8	3336.09	663.42	445.28	162.77	− 12.18
9	3336.57	664.61	445.11	161.66	− 12.35
10	3336.94	665.84	444.95	160.57	− 12.50

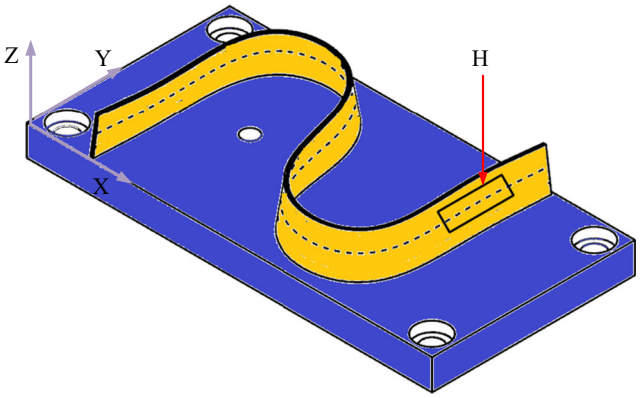

Fig. 8 Schematic diagram of S-shaped specimen

$$St_i = \frac{\sum_{j=M\lambda min}^{N_t} A_j^2}{\sum_{j=1}^{N_t} A_j^2} \tag{15}$$

The variance St_i can be simply viewed as S_i plus all interaction terms of i can express the total influence of error parameter i on the output. Moreover, in order to observe the sensitivity results more intuitively. the global sensitivity index normalization is defined as

$$\overline{St_i} = \frac{1}{N} \sum_{1}^{N} St_i \tag{16}$$

where $\overline{S_i}$ represents the average global sensitivity index of the ith error parameter in the m direction which reflects the total contribution of the single error term (V_i) and coupling error term (V_{ij}) to total error term(V). In addition, it is apparent that the sensitivity index is used to evaluate the contribution of geometric error parameters to position error which has no unit.

Since the sensitivity has been confirmed, there is still one problem that needs to be addressed. It is inevitable to determine the Fourier amplitude of the error parameter to solve the sensitivity coefficient. According to Eq. (8), the geometric error parameters are expressed by truncated Fourier series, and the least square method can be used to determine the Fourier coefficient. For the five-axis machine tool, there are

Fig. 9 S-shaped specimen in processing scene

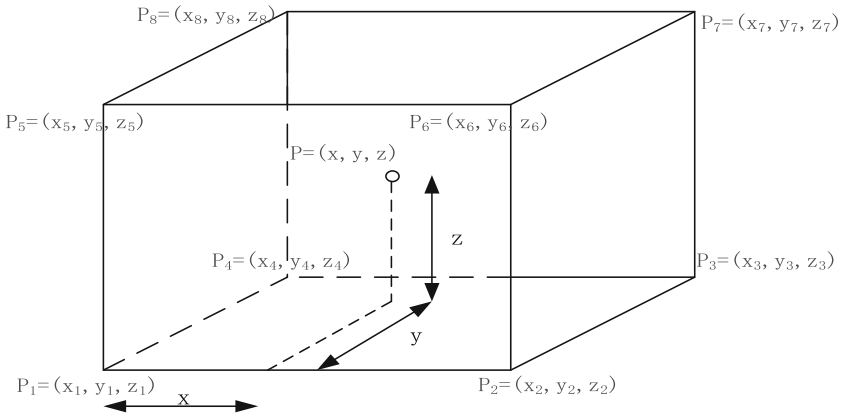

Fig. 10 Linear interpolation compensation value model

30 position-dependent geometric errors. The truncated Fourier coefficients of 30 geometric error parameters are represented by using the row vectors $\boldsymbol{A}_1$, $\boldsymbol{A}_2$, …, $\boldsymbol{A}_{30}$. The parameters in vector **A** are expressed in Eq. (19).

$$A = [A_1, A_2, \ldots, A_{30}] \tag{17}$$

Taking C-axis as an example, the PDGEs are represented by the following.

$$A_i = [A_{i1}, A_{i2}, A_{i3}, A_{i4}, A_{i5}, A_{i6}] \tag{18}$$

$$\begin{cases} \partial_x(c) = \sum_{i=1}^{n} A_{i1} \sin\left(\dfrac{\theta}{2i-1}\right) \\ \partial_y(c) = \sum_{i=1}^{n} A_{i2} \sin\left(\dfrac{\theta}{2i-1}\right) \\ \partial_z(c) = \sum_{i=1}^{n} A_{i3} \sin\left(\dfrac{\theta}{2i-1}\right) \\ \xi_x(c) = \sum_{i=1}^{n} A_{i4} \sin\left(\dfrac{\theta}{2i-1}\right) \\ \xi_y(c) = \sum_{i=1}^{n} A_{i5} \sin\left(\dfrac{\theta}{2i-1}\right) \\ \xi_z(c) = \sum_{i=1}^{n} A_{i6} \sin\left(\dfrac{\theta}{2i-1}\right) \end{cases} \tag{19}$$

Where j(j = 1, 2, ⋯6) is the coefficient of the truncated Fourier polynomials describing the PDGE. n denotes the orders of the polynomials, which are determined by examining the residual errors. (i.e., θ_k= 0).

By transforming Eq. (19), the following equation can be obtained.

$$A^T \theta = B \tag{20}$$

$$\text{Where } A = \begin{bmatrix} A_{11} & A_{21} & A_{31} & A_{41} & A_{51} & A_{61} \\ A_{12} & A_{22} & A_{32} & A_{42} & A_{52} & A_{62} \\ .. & .. & .. & .. & .. & .. \\ A_{1i} & A_{2i} & A_{3i} & A_{4i} & A_{5i} & A_{6i} \\ A_{1n} & A_{2n} & A_{3n} & A_{4n} & A_{5n} & A_{6n} \end{bmatrix}_{n\times 6} \tag{21}$$

$$\theta = \begin{bmatrix} \sin\theta_1 & \sin\theta_2 & \cdots & \sin\theta_j & \sin\theta_k \\ \sin\dfrac{\theta_1}{3} & \sin\dfrac{\theta_2}{3} & \cdots & \sin\dfrac{\theta_j}{3} & \sin\dfrac{\theta_k}{3} \\ \sin\dfrac{\theta_1}{5} & \sin\dfrac{\theta_2}{5} & \cdots & \sin\dfrac{\theta_j}{5} & \sin\dfrac{\theta_k}{5} \\ \cdots\dot{\theta}_1 & \cdots\dot{\theta}_2 & \cdots & \cdots\dot{\theta}_j & \cdots\dot{\theta}_k \\ \sin\dfrac{\theta_1}{2n+1} & \sin\dfrac{\theta_2}{2n+1} & \cdots & \sin\dfrac{\theta_j}{2n+1} & \sin\dfrac{\theta_k}{2n+1} \end{bmatrix}_{n\times k} \tag{22}$$

$$B = \begin{bmatrix} \sigma_x(\theta_1) & \sigma_x(\theta_2) & \ldots & \sigma_x(\theta_j) & \sigma_x(\theta_k) \\ \sigma_y(\theta_1) & \sigma_y(\theta_2) & \ldots & \sigma_y(\theta_j) & \sigma_y(\theta_k) \\ \sigma_z(\theta_1) & \sigma_z(\theta_2) & \ldots & \sigma_z(\theta_j) & \sigma_z(\theta_k) \\ \xi_x(\theta_1) & \xi_x(\theta_2) & \ldots & \xi_x(\theta_j) & \xi_x(\theta_k) \\ \xi_y(\theta_1) & \xi_y(\theta_2) & \ldots & \xi_y(\theta_j) & \xi_y(\theta_k) \\ \xi_z(\theta_1) & \xi_z(\theta_2) & \ldots & \xi_z(\theta_j) & \xi_z(\theta_k) \end{bmatrix}_{6\times k} \tag{23}$$

Thus, the truncated Fourier amplitude of the geometric error parameters can be obtained as

$$A = \left(\theta\theta^T\right)^{-1}\theta B^T \tag{24}$$

Based on the proposed global sensitivity method, the global sensitivity index of each error parameter item can be fully calculated. Then, these sensitivity indexes are sequenced from large to small to find the error parameters that significantly impact the position error of machine tool. Finally, these important geometric errors will be the focus of geometric error

Table 3 Machining error value of S-shaped specimen

S-shaped Specimen	First machining error (mm)	Second machining error (mm)	Reduced	Improved
Processed point 1	0.538	0.419	0.129	22.1%
Processed point 3	0.624	0.486	0.138	22.1%

Fig. 11 The results of two S-shaped specimens

compensation and precision design. For example, suppose each global sensitivity index of error parameters has been calculated by the proposed method. In that case, it can always be found the error parameter with the maximum error sensitivity index comparing the sensitivity index of the remaining error parameters with the maximum error parameter, respectively. Suppose the sensitivity index of an error parameter item is less than one tenth of the maximum error parameter. In that case, it means that the error parameter has little influence on the position error, which can be ignored. If the sensitivity index of an error parameter term is greater than one tenth of the maximum error parameter, it means that the error parameter is regarded as an important error parameter.

4 Simulation and experiment

According to ISO 230 – 6 [19], the tool moves along each body diagonal of the workspace, and the diagonal displacement will be affected by each geometric error. Therefore, eight symmetrical points and one individual center point are selected on the diagonal of two individuals for position error measurement. In the whole motion range of the motion axes, the average position error of the tool at nine points can be simulated, which approximately reflects the influence of geometric error on the whole workspace. Thus, it can be seen from Figs. 5, 6, 7 that the simulation results based on the proposed method. In addition, the histogram comparison is more intuitive, and the vital geometric errors corresponding to larger banded areas are identified. The parameters with more sensitive error in the X direction are sorted in order $\varepsilon_y(y)$, $\varepsilon_y(x)$, $\sigma_x(x)$, $\sigma_x(z)$, $\sigma_x(y)$, $\sigma_x(C)$, $\sigma_x(B)$, $\varepsilon_z(x)$, $\varepsilon_y(z)$. The parameters sensitive to geometric errors in the Y direction are arranged from high to low as follows $\varepsilon_x(y)$, $\varepsilon_x(x)$, $\sigma_y(z)$, $\sigma_y(x)$, $\sigma_y(y)$, $\sigma_y(B)$, $\sigma_y(C)$, $\varepsilon_x(z)$, and the vital geometric error parameters that affect the position error of machine tool in the Z direction are $\sigma_z(z)$, $\varepsilon_z(x)$, $\sigma_z(y)$, $\sigma_z(B)$, $\varepsilon_x(x)$, $\varepsilon_y(x)$, $\varepsilon_y(y)$. According to the sensitivity results, the unidirectional error is significantly affected by $\varepsilon_y(y)$the straightness error in general. For example, the sensitive straightness error parameters in the Z direction are$\sigma_z(C)$ and $\sigma_z(z)$. Moreover, the most sensitive error parameters in the X and Y directions are the angle error such as $\varepsilon_y(y)$, $\varepsilon_y(x)$, $\varepsilon_x(y)$, $\varepsilon_x(x)$, respectively. In addition, these more sensitive geometric error parameters in all directions are vital geometric error parameters that affect the machining accuracy of the machine tool. From the

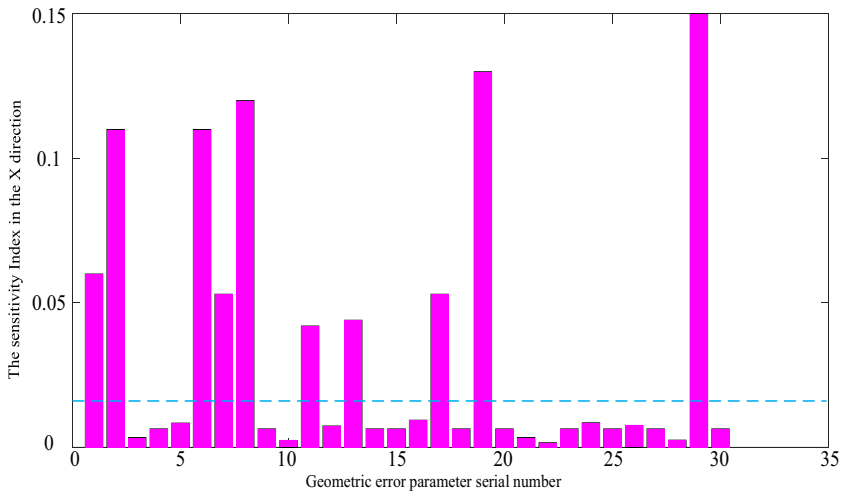

Fig. 12 Global sensitivity index in the X direction

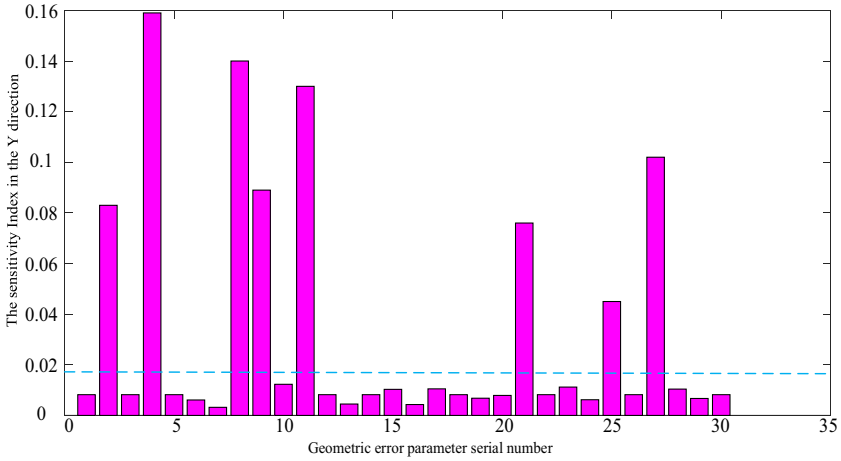

Fig. 13 Global sensitivity index in the Y direction

sensitivity analysis results, the angle error parameters have a great influence on the position error of the machine tool. At the same time, the straightness error parameters and angle error parameters related to the translational axis have a significant effect on the position error of the machine tool, which may be because the translational axis is at the top of the machine tool motion chain.

The machining error of machine tool is affected by many factors. Reducing the position error of machine tool is an effective means to improve the machining accuracy. Thus, in order to verify the validity of the proposed method, error compensation experiments are performed to compensate the vital geometric errors. The experiment is divided into two steps. The first step is that the S-shaped specimen is machined in the five-axis gantry machine. After that, the coordinate measuring machine is used to detect machining accuracy of the S-shaped specimen. The second step: After the obtained vital geometric error parameter items are compensated, the S-shaped specimen is conducted to machined in this improved machine tool. Then, the validity of the sensitivity method was proved by comparing the machining accuracy of two S-shaped specimens. The purpose of the second experiment is aimed to prove that the vital geometric error parameters obtained by the proposed sensitivity analysis method play important roles in the improvement of machine tool machining accuracy. In Section 2, the workspace of the five-axis machine tool has been introduced. As displayed in Fig. 8, the S-shaped specimen of which upper and lower directrix is a continuous b-spline curve fitting by using the second derivative is used to test the machining accuracy of five-axis machine tools. The S-shaped specimen's length, width, height, and thickness are 250 mm, 175 mm, 40 mm, and 3 mm, respectively. However, as the machining track of S-shaped specimen is a surface, according to Ref. [20], it introduces Frenet frame to represent surface machining error more accurately by deviations of tangential direction, normal direction, and binormal direction instead of X, Y, and Z directions. The processing scene of S-shaped specimen is shown in Fig. 9. Therefore, the normal direction of error increment is considered as an important indicator to verify the machining accuracy. Moreover, in order to avoid the theoretical error caused by the distortion angle of the S-shaped specimen, the region H is selected as the processing region. In addition, since there are numerous cutting tool positions in the machining process, 10 sampling points are selected to reflect the cutting tool

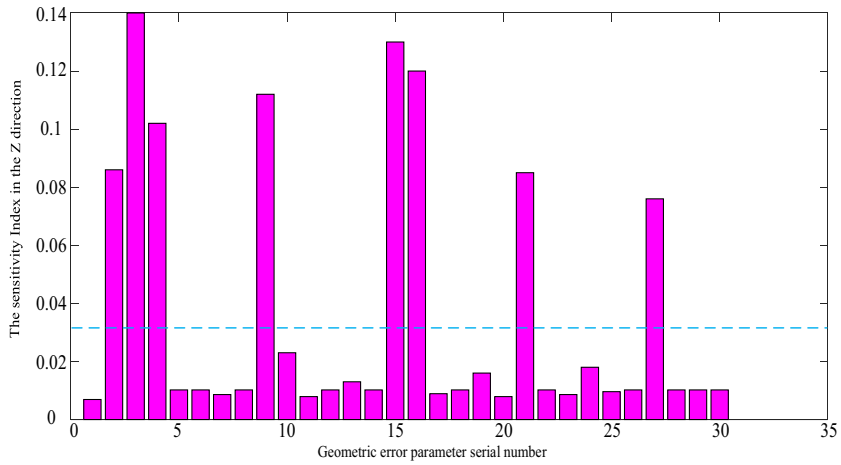

Fig. 14 Global sensitivity index in the Z direction

positions in Table 2 effectively. According to a Latin hypercube sampling technique in each data acquisition point, for each position of the geometric error, each point 700 data were acquired. In Section 3 (0.1 μm for the position errors and 0.1 μrad for the angular errors), the global sensitivity index for each geometric error can be calculated by Eq. (20).

The linear interpolation method was used to compensate the vital geometric error parameters to observe the machining accuracy after compensation. The geometric errors of the translation axis are identified by the laser interferometer, and the geometric errors of the rotation axis are identified by double ball bar. The identification results of geometric errors are illustrated in Appendix 2. The compensated values of vital geometric errors are generated by the postprocessor to generate NC code to modify the tool position. This paper makes use of the position error compensation function module provided by the commercial numerical control system (FANUC), where an external compensator is added based on the original numerical control system. The compensation principle is as follows.

The position error space is divided into several cuboid grids, and the number of nodes in X, Y, and Z directions is denoted as M_x, M_y, and M_z, respectively. Considering the storage problem, the grid nodes should be selected appropriately. When the machine tool moves to any point P in the workspace, a cuboid element can always be found with the point P located inside or on the boundary. The cuboid vertices and their seats are marked $P_j=(x_j,y_j,z_j)$ (j=8). As illustrated in Fig. 10, it can be seen that linear interpolation of any point in a unit. In order to explain clearly, the X-direction deviation is taken as the compensation object, where Δp_x represents the value of the linear interpolation compensation method.

$$\Delta p_x = \sum_{j=i}^{8} c_j \Delta p_{xj} \tag{25}$$

$$\begin{cases} c_1 = (1-k_x)(1-k_y)(1-k_z), c_2 = k_x(1-k_y)(1-k_z), c_3 = k_x k_y(1-k_z) \\ c_4 = (1-k_x)k_y(1-k_z), c_5 = (1-k_x)(1-k_y)k_z, c_6 = k_x(1-k_y)k_z \\ c_7 = k_x k_y k_z, c_8 = (1-k_x)k_y k_z \end{cases} \tag{26}$$

In the formula above, k_x, k_y and k_z represent normalized internal fraction ratios of point P in the X, Y and Z directions, respectively. The values of k_i are distributed between 0 and 1, which can be obtained by interpolation arithmetic.

$$k_x = \frac{|x-x_1|}{|x_2-x_1|}, k_y = \frac{|y-y_1|}{|y_4-y_1|}, k_z = \frac{|z-z_1|}{|z_5-z_1|} \tag{27}$$

Since the Y and Z direction compensation methods are the same, there is no need to repeat them here. The corresponding compensation values of all mesh nodes are uploaded to the numerical control system to compensate for the position error.

After compensating for the vital geometric error of machine tool, another S-shaped specimen was processed. Then, it was tested by a coordinate measuring machine. The results of two S-shaped specimens processed are illustrated in Fig. 11, where the surface quality before compensation is significantly worse than that after compensation. Moreover, the results show that the machining error is significantly reduced. As illustrated in Table 3, the machining error values of processed point 1 and 3 before compensation are measured as 0.583 mm and 0.624 mm, respectively. When the five-axis machine tool has been compensated by the linear interpolation compensation, the machining error value of S-shaped specimen in processed point 1 was reduced by 0.129 mm, which improved the machining accuracy by 22.1%. Similarly, when the machining error value of machining point 3 was obtained, the machining error was reduced by 0.122 compared with the first one, which improved the machining accuracy by 22.1%. It means that the machining accuracy of the machine tool has been significantly improved by compensating the vital geometric error parameters. In addition, the sensitivity indexes of the geometric error are calculated by the proposed sensitivity method. It can be seen from Fig. 12, Fig. 13, and Fig. 14 that the second sensitivity analysis has made a noticeable difference compared with the first one. The sensitivity indexes of vital geometric error parameters have been reduced significantly, which are still the vital geometric error parameters that affect the machining accuracy of the machine tool compared with other error parameters. The compensation result indicates that reducing the vital geometric errors has obvious benefits to improve the machining accuracy. However, the sensitivity indexes of geometric error parameters $\varepsilon_x(x)$, $\varepsilon_z(x)$, $\sigma_x(B)$, $\sigma_z(B)$, $\varepsilon_y(C)$ have increased, which may be caused by geometric error parameters coupling results. In summary, the influence of vital geometric error parameters on the machining accuracy of the machine tool is reduced by linear interpolation compensation. Thus, it can be reasonably concluded that the proposed sensitivity analysis method is accurate and feasible.

5 Conclusion

In this paper, the proposed method is first used to establish the position error model of the five-axis planer milling machine tool and then to deduce the sensitivity analysis model for five-axis machine tool. Moreover, the vital geometric errors of the machine tool are identified, which provides an important theoretical basis for the design of machine tool. Finally, the machining accuracy of machine tool has been significantly improved by compensating the vital geometric errors.

Above all, the following areas need to be studied in the future.

(1) In this paper, the geometric error modeling and machining precision solving methods of machine tools are studied without considering cutting force and thermal error. Therefore, factors such as cutting force and cutting heat error can be considered in the study of machining accuracy in the future

(2) The geometric error item may be sensitive to some points and insensitive to some processing points. Therefore, how to calculate the interval sensitivity of geometric error terms has important practical significance for further research.

Appendix 1

Table 4 Position transformation matrix between adjacent bodies

	Ideal position matrix	Position error matrix
0-1 (X-axis)	$[T01]_{\mathrm{p}} = \begin{bmatrix} 1 & 0 & 0 & q_{2\mathrm{x}} \\ 0 & 1 & 0 & q_{2\mathrm{y}} \\ 0 & 0 & 1 & q_{2\mathrm{z}} \\ 0 & 0 & 0 & 1 \end{bmatrix}$	$[T01]_{\mathrm{pe}} = E_{4\times4}$
1-2 (Y-axis)	$[T12]_{\mathrm{p}} = \begin{bmatrix} 1 & 0 & 0 & q_{3\mathrm{x}} \\ 0 & 1 & 0 & q_{3\mathrm{y}} \\ 0 & 0 & 1 & q_{3\mathrm{z}} \\ 0 & 0 & 0 & 1 \end{bmatrix}$	$[T12]_{\mathrm{pe}} = \begin{bmatrix} 1 & 0 & S_{\mathrm{xz}} & 0 \\ 0 & 1 & -S_{\mathrm{yz}} & 0 \\ -S_{\mathrm{xz}} & S_{\mathrm{yz}} & 1 & 0 \\ 0 & 0 & 0 & 1 \end{bmatrix}$
2-3 (Z-axis)	$[T23]_{\mathrm{p}} = \begin{bmatrix} 1 & 0 & 0 & q_{4\mathrm{x}} \\ 0 & 1 & 0 & q_{4\mathrm{y}} \\ 0 & 0 & 1 & q_{4\mathrm{z}} \\ 0 & 0 & 0 & 1 \end{bmatrix}$	$[T23]_{\mathrm{pe}} = \begin{bmatrix} 1 & 0 & S_{\mathrm{xz}} & 0 \\ 0 & 1 & -S_{\mathrm{yz}} & 0 \\ -S_{\mathrm{xz}} & S_{\mathrm{yz}} & 1 & 0 \\ 0 & 0 & 0 & 1 \end{bmatrix}$
3-4 (C-axis)	$[T34]_{\mathrm{p}} = \begin{bmatrix} 1 & 0 & 0 & q_{5\mathrm{x}} \\ 0 & 1 & 0 & q_{5\mathrm{y}} \\ 0 & 0 & 1 & q_{5\mathrm{z}} \\ 0 & 0 & 0 & 1 \end{bmatrix}$	$[T34]_{\mathrm{pe}} = \begin{bmatrix} 1 & 0 & S_{\mathrm{xc}} & 0 \\ 0 & 1 & -S_{\mathrm{yc}} & 0 \\ -S_{\mathrm{xc}} & S_{\mathrm{yc}} & 1 & 0 \\ 0 & 0 & 0 & 1 \end{bmatrix}$
4-5 (B-axis)	$[T45]_{\mathrm{p}} = \begin{bmatrix} 1 & 0 & 0 & q_{6\mathrm{x}} \\ 0 & 1 & 0 & q_{6\mathrm{y}} \\ 0 & 0 & 1 & q_{6\mathrm{z}} \\ 0 & 0 & 0 & 1 \end{bmatrix}$	$[T45]_{\mathrm{pe}} = \begin{bmatrix} 1 & -S_{\mathrm{bz}} & 0 & 0 \\ S_{\mathrm{bz}} & 1 & -S_{\mathrm{xb}} & 0 \\ 0 & S_{\mathrm{xb}} & 1 & 0 \\ 0 & 0 & 0 & 1 \end{bmatrix}$

Table 5 Position motion transformation matrix between adjacent bodies

	Ideal motion matrix	Motion error matrix
0-1(X-axis)	$[T01]_{\mathrm{s}} = \begin{bmatrix} 1 & 0 & 0 & x \\ 0 & 1 & 0 & 0 \\ 0 & 0 & 1 & 0 \\ 0 & 0 & 0 & 1 \end{bmatrix}$	$[T01]_{\mathrm{se}} = [1\ \ -\varepsilon_{\mathrm{z}}(x)\ \ \varepsilon_{\mathrm{y}}(x)\ \ \sigma_{\mathrm{x}}(x)\varepsilon_{\mathrm{z}}(x)\ \ 1-\varepsilon_{\mathrm{x}}(x)\ \ \sigma_{\mathrm{y}}(x)-\varepsilon_{\mathrm{y}}(x)\ \ \varepsilon_{\mathrm{x}}(x)\ \ 1\sigma_{\mathrm{z}}(x)0\ 001]$
1-2 (Y-axis)	$[T12]_{\mathrm{s}} = \begin{bmatrix} 1 & 0 & 0 & 0 \\ 0 & 1 & 0 & y \\ 0 & 0 & 1 & 0 \\ 0 & 0 & 0 & 1 \end{bmatrix}$	$[T12]_{\mathrm{se}} = [1\ \ -\varepsilon_{\mathrm{z}}(y)\ \ \varepsilon_{\mathrm{y}}(y)\ \ \sigma_{\mathrm{x}}(y)\varepsilon_{\mathrm{z}}(y)\ \ 1-\varepsilon_{\mathrm{x}}(y)\ \ \sigma_{\mathrm{y}}(y)-\varepsilon_{\mathrm{y}}(y)\ \ \varepsilon_{\mathrm{x}}(y)\ \ 1\sigma_{\mathrm{z}}(y)0\ 001]$
2-3 (Z-axis)	$[T23]_{\mathrm{s}} = \begin{bmatrix} 1 & 0 & 0 & 0 \\ 0 & 1 & 0 & 0 \\ 0 & 0 & 1 & z \\ 0 & 0 & 0 & 1 \end{bmatrix}$	$[T23]_{\mathrm{se}} = [1\ \ -\varepsilon_{\mathrm{z}}(z)\ \ \varepsilon_{\mathrm{y}}(z)\ \ \sigma_{\mathrm{x}}(z)\varepsilon_{\mathrm{z}}(z)\ \ 1-\varepsilon_{\mathrm{x}}(z)\ \ \sigma_{\mathrm{y}}(z)-\varepsilon_{\mathrm{y}}(z)\ \ \varepsilon_{\mathrm{x}}(z)\ \ 1\sigma_{\mathrm{z}}(z)00\ 01]$
3-4 (C-axis)	$[T34]_{\mathrm{s}} = [\cos(c)\ \ -\sin(c)\ 00\sin(c)\ \cos(c)\ 00001000\ 01]$	$[T34]_{\mathrm{se}} = [1\ \ -\varepsilon_{\mathrm{z}}(c)\ \ \varepsilon_{\mathrm{y}}(c)\ \ \sigma_{\mathrm{x}}(c)\varepsilon_{\mathrm{z}}(c)\ \ 1-\varepsilon_{\mathrm{x}}(c)\ \ \sigma_{\mathrm{y}}(c)-\varepsilon_{\mathrm{y}}(c)\ \ \varepsilon_{\mathrm{x}}(c)\ \ 1\sigma_{\mathrm{z}}(c)0\ 001]$
4-5 (B-axis)	$[T45]_{\mathrm{s}} = [\cos(b)\ \ 0\sin(b)\ 00100-\sin(b)\ 0\cos(b)\ 00\ 001]$	$[T45]_{\mathrm{se}} = [1\ \ -\varepsilon_{\mathrm{z}}(b)\ \ \varepsilon_{\mathrm{y}}(b)\ \ \sigma_{\mathrm{x}}(b)\varepsilon_{\mathrm{z}}(b)\ \ 1-\varepsilon_{\mathrm{x}}(b)\ \ \sigma_{\mathrm{y}}(b)-\varepsilon_{\mathrm{y}}(b)\ \ \varepsilon_{\mathrm{x}}(b)\ \ 1\sigma_{\mathrm{z}}(b)\ 0001]$

Appendix 2

$$\delta_x(x) = \frac{-0.0129x}{5000} + 0.0046\sin\left(\frac{2.2633\pi x}{5000} - 0.6332\right)$$

$$\delta_y(x) = 0.0296\sin\left(\frac{2.5828\pi x}{5000} + 1.4918\right) + 0.4288\sin\left(\frac{5.0024\pi x}{5000} - 3.3295\right) + 0.4245\sin\left(\frac{5.0331\pi x}{5000} - 0.2304\right)$$

$$\delta_z(x) = 0.0376\sin\left(\frac{0.0136\pi x}{5000} + 3.0638\right) + 0.0124\sin\left(\frac{2.6840\pi x}{5000} + 3.5962\right) + 0.0145\sin\left(\frac{6.2096\pi x}{5000} + 2.3885\right)$$

$$\varepsilon_z(x) = 2.9529 \times 10^{-5}\sin\left(\frac{0.5271\pi x}{5000} + 2.7075\right) + 7.4715 \times 10^{-6}\sin\left(\frac{4.3723\pi x}{5000} + 2.9819\right) + 7.7088 \times 10^{-6}\sin\left(\frac{7.4411\pi x}{5000} - 0.5413\right)$$

$$\varepsilon_y(x) = 2.9990 \times 10^{-6}\sin\left(\frac{2.0054\pi x}{5000} + 2.4608\right) + 4.1933 \times 10^{-17}\sin\left(\frac{3.5549\pi x}{5000} + 0.2324\right) + 7.3236 \times 10^{-6}\sin\left(\frac{6.000\pi x}{5000} - 0.9056\right)$$

$$\varepsilon_x(x) = 1.0384 \times 10^{-4}\sin\left(\frac{0.1089\pi x}{5000} + 5.9992\right) + 2.7342 \times 10^{-5}\sin\left(\frac{0.6971\pi x}{5000} + 2.0011\right) + 3.4038 \times 10^{-6}\sin\left(\frac{4.7893\pi x}{5000} + 1.9626\right)$$

Authors contribution Jinwei Fan and Peitong Wang provided ideas for this study, wrote codes and manuscripts. Xingfei Ren were responsible for the experiment in this study. All authors contributed to this study.

Funding This work is financially supported by the National Natural Science Foundation of China (grant No. 51775010 and 51705011), the National Science and Technology Major Project of China (grant No. 2019ZX040 06001).

Data availability The authors confirm that the data supporting the findings of this study are available within the article.

Code availability The authors confirm that the code supporting the findings of this study are available within the article.

Declarations

Ethics approval The research does not involve ethical issues.

Consent for publication All the authors agreed to publish this paper.

Competing interests The authors declare no competing interests.

References

1. Fan JW, Tang YH, Chen DJ, Wu CJ (2017) A geometric error tracing method based on the Monte Carlo theory of the five-axis gantry machining center. Adv Mech Eng 9(7):1–14
2. Liu Y, Wan M, Xing W-J, Zhang W-H (2018) Identification of position independent geometric errors of rotary axis for five-axis machine tools with structural restrictions. Robot Comput Integr Manuf 53:45–57
3. Ramesh R, Mannan MA, Poo AN (2000) Error compensation in machine tools —a review: Part I: geometric, cutting-force induced and fixture-dependent errors. Int J Mach Tools Manuf 40:1235–1256
4. Bryan JB (1982) A simple method for testing measuring machines and machine tools part 1: principles and applications. Precis Eng 4:61–69
5. Tsutsumi M, Saito A (2003) Identification and compensation of systematic deviations particular to 5-axis machining centers. Int J Mach Tools Manuf 43:771–780

6. Ibaraki S, Oyama C, Otsubo H (2011) Construction of an error map of rotary axis on a five-axis machining center by static R-test. Int J Mach Tools Manuf 51:190–200
7. Fu G, Fu J, Gao H, Yao X (2017) Squareness error modeling for five-axis machine tools via synthesizing the motion of the axis. Int J Adv Manuf Technol 89(9):2993–3008
8. Chen GS, Mei XS, Li HL (2013) Geometric error modeling and compensation for large-scale grinding machine tools with five-axis. Int J Adv Manuf Technol 69(9–12):2583–2592
9. Lee JH, Liu Y, Yang SH (2006) Accuracy improvement of miniaturized machine tool: geometric error modeling and compensation. Int J Mach Tools Manuf 46(12–13):1508–1516
10. Zhu S, Ding G, Qin S, Lei J, Zhuang L, Yan K (2012) Integrated geometric error modeling, identification and compensation of CNC machine tools. Int J Mach Tools Manuf 52(1):24–29
11. Zhu W, Wang Z, Yamazaki K (2010) Machine tool component error extraction and error compensation by incorporating statistical analysis. Int J Mach Tools Manuf 50(1):798–806
12. Zhang H, Yang J, Zhang Y, Shen J, Wang C (2011) Measurement and compensation for volumetric positioning errors of CNC machine tools considering thermal effect. Int J Adv Manuf Technol 55(1):275–283
13. He Z, Fu J, Zhang X, Shen H (2016) A uniform expression model for volumetric errors of machine tools. Int J Mach Tools Manuf 100:93–104
14. Zhang X, Zhang Y, Pandey MD (2015) Global sensitivity analysis of a CNC machine tool : application of MDRM. Int J Adv Manuf Technol 81(1–4):159–169
15. Huang T, Li Y, Tang GB, Li SW, Zhao XY, White House DJ, Chetewyn DG, Liu XP (2002) Error modeling, sensitivity analysis and assembly process of a class of 3-DOF parallel kinematic machines with parallelogram struts. Sci China (Series E) 45(5):467–476
16. Huang P (2011) Research on the accuracy assurance of a class of 3-DOF spacial parallel manipulators. Tsinghua University, China
17. Xing K, Achiche S, Mayer JRR (2019) Five-axis machine tools accuracy condition monitoring based on volumetric errors and vector similarity measures. Int J Mach Tools Manuf 138:80–93
18. Li Q (2018) A sensitivity method to analyze the volumetric error of five-axis machine tool. Int J Adv Manuf Technol 98:1791–1805
19. International Standards Organization (ISO) (2002) ISO 230–6: test code for machine tools, Part 6: determination of positioning accuracy on body and face diagonals (Diagonal displacement tests)
20. Li Z, Sato R, Shirase K, Ihara Y, Milutinovic DS (2019) Sensitivity analysis of relationship between error motions and machined shape errors in five-axis machining center — peripheral milling using square end mill as test case. Precis Eng 60:28–41